Inorganic Chemistry
Article

Inorg. Chem. **2009**, *48*, 10507–10511 **10507**
DOI: 10.1021/ic900777g

Photon-Driven Catalytic Proton Reduction with a Robust Homoleptic Iridium(III) 6-Phenyl-2,2′-bipyridine Complex ($[Ir(C^{\wedge}N^{\wedge}N)_2]^+$)

Leonard L. Tinker and Stefan Bernhard*

Department of Chemistry, Princeton University, Princeton, New Jersey 08544

Received April 22, 2009

The improved stability of a photocatalytic proton reduction system is accomplished when a heteroleptic *bis*-cyclometalated diimine iridium(III) photosensitizer ($[Ir(ppy)_2(bpy)]^+$, ppy=2-phenylpyridine and bpy=2,2′-bipyridine) is replaced with a novel iridium complex, $[Ir(phbpy)_2]^+$ (phbpy = 6-phenyl-2,2′-bipyridine). The decomposition of $[Ir(ppy)_2(bpy)]^+$ analogs in photocatalytic systems has been previously shown to result from 2,2′-bipyridine dissociation, which will be hindered by the improved architecture. Although desirable for reasons beyond stability, syntheses of *bis*-tridentate iridium complexes of 6-phenyl-2,2′-bipyridine are uncommon, with no previous examples having an analogous coordination sphere to the well-studied $[Ir(C^{\wedge}N)_2(N^{\wedge}N)]^+$ architecture (where $C^{\wedge}N$ = cyclometalating ligand and $N^{\wedge}N$ = neutral diimine ligand). Ligand modification has proven a successful strategy in tuning the photophysical properties of $[Ir(C^{\wedge}N)_2(N^{\wedge}N)]^+$ complexes and can now be employed for the more robust $[Ir(C^{\wedge}N^{\wedge}N)_2]^+$ framework (where $C^{\wedge}N^{\wedge}N$ = cyclometalating diimine ligand). Characterization of the novel complex reveals similar electrochemical properties and calculated orbital densities to the parent $[Ir(ppy)_2(bpy)]^+$ species, while there are notable differences between the absorption and photophysical properties of the two complexes.

Introduction

Luminescent transition metal complexes have a high degree of utility in a variety of fields including organic light-emitting devices (OLEDs), solar energy conversion, and optical sensing.[1−3] Such applications rely on the complex's electronically excited states, which can be adjusted through metal selection and ligand design. The versatility of the electronically excited state is often dependent on its lifetime, and therefore, the propagation of a long-lived triplet state is advantageous. As a result, heavy atoms with enhanced spin−orbit coupling are typically selected. Even in applications where the lifetime of the excited state is not a key parameter, such as OLED emitters, there are still advantages in facilitating singlet−triplet interconversion due to an increased quantum efficiency of electroluminescence.[4] As a consequence of these ideal properties, *tris*-diimine complexes of ruthenium(II) ($[Ru(N^{\wedge}N)_3]^{2+}$) have been extensively studied as chromophores for a specific OLED known as a light-emitting electrochemical cell, and for light-to-chemical energy conversion schemes.[5−9] However, it was ultimately realized that the tuning of the excited states of $[Ru(N^{\wedge}N)_3]^{2+}$ complexes was hindered due to the thermal population of a dissociative and energetically limiting ^{3}MC state.[10−12] When used as an emitter, the detrimental effect of the dissociative ^{3}MC state is further amplified since the decomposition products can be effective excited state quenchers, therefore, accelerating device degradation.[13,14] To solve this issue, researchers moved to heavier atoms with increased ligand field stabilization energies and a consequently less accessible ^{3}MC state.[15] Recently, heteroleptic cyclometalated complexes of the general structure $[Ir(C^{\wedge}N)_2(N^{\wedge}N)]^+$ ($C^{\wedge}N$ = cyclometalating ligand such as 2-phenylpyridine) have gained attention, as the increased energy of the ^{3}MC state allows for a greater range of luminescence energies.[1] In addition, the mixing of the ligand-centered (LC) and metal-to-ligand

*Phone: 609-258-3879 Fax: 609-258-6746 bern@princeton.edu.

(1) Lowry, M. S.; Bernhard, S. *Chem.—Eur. J.* **2006**, *12*(31), 7970–7977.
(2) Demas, J. N.; DeGraff, B. A. *Coord. Chem. Rev.* **2001**, *211*, 317–351.
(3) Tinker, L. L.; McDaniel, N. D.; Bernhard, S. *J. Mater. Chem.* **2009**, DOI: 10.1039/b818112h.
(4) Thompson, M. E.; Burrows, P. E.; Forrest, S. R. *Curr. Opin. Solid State Mater. Sci.* **1999**, *4*(4), 369–372.
(5) Juris, A.; Balzani, V.; Barigelletti, F.; Campagna, S.; Belser, P.; Von Zelewsky, A. *Coord. Chem. Rev.* **1988**, *84*, 85–277.
(6) Bernhard, S.; Barron, J. A.; Houston, P. L.; Abruña, H. D.; Ruglovksy, J. L.; Gao, X.; Malliaras, G. G. *J. Am. Chem. Soc.* **2002**, *124* (45), 13624–13628.
(7) Kalyanasundaram, K. *Coord. Chem. Rev.* **1982**, *46*, 159–244.
(8) Lee, J.-K.; Yoo, D. S.; Handy, E. S.; Rubner, M. F. *Appl. Phys. Lett.* **1996**, *69*(12), 1686–1688.
(9) Tokel-Takvoryan, N. E.; Hemingway, R. E.; Bard, A. J. *J. Am. Chem. Soc.* **1973**, *95*(20), 6582–6589.
(10) Durham, B.; Caspar, J. V.; Nagle, J. K.; Meyer, T. J. *J. Am. Chem. Soc.* **1982**, *104*(18), 4803–4810.
(11) Harrigan, R. W.; Crosby, G. A. *J. Chem. Phys.* **1973**, *59*(7), 3468–3476.
(12) Van Houten, J.; Watts, R. J. *J. Am. Chem. Soc.* **1976**, *98*(16), 4853–4858.
(13) Soltzberg, L. J.; Slinker, J. D.; Flores-Torres, S.; Bernards, D. A.; Malliaras, G. G.; Abruna, H. D.; Kim, J. S.; Friend, R. H.; Kaplan, M. D.; Goldberg, V. *J. Am. Chem. Soc.* **2006**, *128*(24), 7761–7764.
(14) Kalyuzhny, G.; Buda, M.; McNeill, J.; Barbara, P.; Bard, A. J. *J. Am. Chem. Soc.* **2003**, *125*(20), 6272–6283.
(15) Watts, R. J.; Crosby, G. A. *J. Am. Chem. Soc.* **1971**, *93*(13), 3184–3188.

Published on Web 07/16/2009

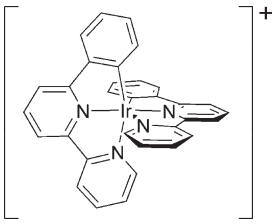

Figure 1. Structural representation of $[Ir(phbpy)_2]^+$ that is synthesized and used in catalytic proton reduction systems in this report.

charge-transfer (MLCT) states[16,17] further facilitates the manipulation of the electronically excited state through ligand design since the LC transition is associated with the cyclometalating ligand, while the MLCT transition can be adjusted through the modification of the ancillary (N^N) group.[18]

By altering the framework of the $[Ir(C^N)_2(N^N)]^+$ complexes to a system such as $[Ir(C^N^N)_2]^+$ (Figure 1), a more rigid and substitution-inert complex is obtained without affecting the ligand sphere around the iridium(III) center. The use of a tridentate ligand may strain the octahedral geometry, which could lead to a decreased emission quantum yield and excited state lifetime, as seen in the comparison between $[Ru(bpy)_3]^{2+}$ and $[Ru(tpy)_2]^{2+}$ (tpy = 2,2′:6′,2″-terpyridine).[5,19,20] However, there are multiple additional advantages in the use of tridentate ligands such as photophysical effects, isomer isolation, and facile incorporation into a linear assembly.[21,22] A variety of iridium(III) complexes of tridentate ligands have been previously reported using (N^N^N), (C^N^C), and (N^C^N) coordinating ligands,[21−23] but this is the first description of a homoleptic complex having a similar coordination environment to that of the highly versatile $[Ir(C^N)_2(N^N)]^+$ architecture with cis bonds to phenyl moieties. Previously reported *bis*-(C^N^N) iridium complexes are complexes of 2,2′:6′,2″-terpyridine analogues with cyclometalating bonds to a pyridine moiety,[24,25] and therefore, have a different electronic structure than the $[Ir(C^N)_2(N^N)]^+$ complexes with cyclometalated phenyl moieties. Additionally, the synthesis and isolation of an $[Ir(C^N^N)_2]^+$ complex is complicated by a variety of ligand binding modes and are frequently reported to coordinate in a bidentate fashion.[21] Tridentate 6-phenyl-2,2′-bipyridine (phbpy) ligands can conveniently be synthesized through a variety of methods that allow for the independent modification of phenyl and pyridine subunits, and thus, the excited states of the resulting complexes can be altered using the same strategies employed for the $[Ir(C^N)_2(N^N)]^+$ architecture. Herein, the synthesis of $[Ir(phbpy)_2]PF_6$ is described, as well as demonstrating its enhanced stability as a photosensitizing complex in catalytic hydrogen-producing systems.

Experimental Section

General. ^1H and ^{13}C NMR were recorded on a Bruker BioSpin Avance II 500 MHz spectrometer. UV−vis spectra were recorded using a Hewlett-Packard 8453 diode-array spectrophotometer. Mass spectral (MS) data were collected on a Hewlett-Packard 5898B electrospray engine. Emission spectra were recorded using a Jobin-Yvon Fluorolog-3 spectrometer equipped with double monochromators and a Hamamatsu-928 photomultiplier tube at right-angle geometry. 20 μM solutions in acetonitrile (ACN) were prepared for lifetime measurements and were degassed by bubbling with ACN-saturated N_2 for 10 min. Lifetime data were recorded using a Tektronix TDS 3032B digital phosphor oscilloscope after excitation at 337 nm with a Laser Science VSL-337LRF N_2 laser using a 10 ns pulse, and emission quantum yields (Φ_{em}) were calculated relative to a $[Ru(bpy)_3](PF_6)_2$ reference ($\Phi_r = 0.0620$).[26] Cyclic voltammetry (CV) was performed on a CH-Instruments Electrochemical Analyzer 600C potentiostat using a 1 mm^2 platinum disk working electrode, a coiled platinum wire supporting electrode, and a silver wire as a pseudoreference electrode. Ferrocene was employed as an internal standard, and its Fe(II/III) half-wave potential was taken to be 370 mV against the standard calomel electrode (SCE). The 500 μM solutions of $[Ir(phbpy)_2]PF_6$ and $[Ir(ppy)_2(bpy)]PF_6$ were prepared in ACN containing 0.1 M tetra-*n*-butylammonium hexafluorophosphate (TBAH). The samples were degassed by bubbling ACN-saturated N_2 into the solution for 10 min before the voltammograms were recorded at a 100 mV/s sweep rate. Elemental analyses were conducted by the Microanalytical Laboratory at the University of Illinois, Urbana−Champaign.

Materials and Reagents. $IrCl_3 \cdot 4H_2O$ was purchased from Pressure Chemical Company, while all other reagents and solvents were used without further purification except for the tetrahydrofuran used for the photoreactions that was distilled over sodium and benzophenone just before use. The phbpy ligand was synthesized as previously reported.[27]

Synthesis of $[Ir(phbpy)_2]PF_6$. $IrCl_3 \cdot 4H_2O$ (363 mg, 0.98 mmol) was combined with phbpy (455 mg, 1.96 mmol) in ethylene glycol (14 mL), and the reaction mixture was heated at 175 °C for 90 h. The reaction mixture was then cooled and diluted with water (200 mL), and the aqueous solution was washed with ether (2 × 60 mL). The product was extracted into dichloromethane (200 mL) that was washed with water (50 mL). The combined aqueous phases were extracted again with dichloromethane (2 × 200 mL). The combined organic extracts were concentrated under reduced pressure, and the residue was extracted with 70 °C water (500 mL) for 15 min. The hot aqueous solution was clarified by filtration through a sinterted glass frit, and the product was precipitated by the addition of a 0.5 M aqueous solution of NH_4PF_6 (4.0 mL). The solution was cooled to 5 °C for 16 h, and the crude product was isolated by vacuum filtration, washed with water (2 × 20 mL), and dried under reduced pressure to give a dark red powder (360 mg, 0.46 mmol). To ensure sufficient product purity for analysis as a photosensitizer in H_2-forming reactions, the crude product was then dry-loaded onto silica (5 g) using acetone and eluded through a 4 × 46 cm silica column with a 6 mM NH_4PF_6 solution in 8:1 ethanol/water. A series of pure fractions was identified by ^1H NMR and combined to give a net volume of ∼400 mL. The combined fractions were reduced to approximately 25% volume under

(16) Colombo, M. G.; Hauser, A.; Güdel, H. U. *Inorg. Chem.* **1993**, *32* (14), 3088–3092.
(17) Colombo, M. G.; Hauser, A.; Güdel, H. U. *Top. Curr. Chem.* **1994**, *171*, 143–171.
(18) Lowry, M. S.; Hudson, W. R.; Pascal, R. A.; Bernhard, S. *J. Am. Chem. Soc.* **2004**, *126*(43), 14129–14135.
(19) Sauvage, J. P.; Collin, J. P.; Chambron, J. C.; Guillerez, S.; Coudret, C.; Balzani, V.; Barigelletti, F.; De Cola, L.; Flamigni, L. *Chem. Rev.* **1994**, *94*(4), 993–1019.
(20) Hecker, C. R.; Gushurst, A. K. I.; McMillin, D. R. *Inorg. Chem.* **1991**, *30*(3), 538–541.
(21) Bexon, A. J. S.; Williams, J. A. G. *C. R. Chim.* **2005**, *8*(8), 1326–1335.
(22) Williams, J. A. G.; Wilkinson, A. J.; Whittle, V. L. *Dalton Trans.* **2008**, No. 16, 2081–2099.
(23) Whittle, V. L.; Williams, J. A. G. *Inorg. Chem.* **2008**, *47*(15), 6596–6607.
(24) Mamo, A.; Stefio, I.; Parisi, M. F.; Credi, A.; Venturi, M.; DiPietro, C.; Campagna, S. *Inorg. Chem.* **1997**, *36*(25), 5947–5950.
(25) Di Marco, G.; Lanza, M.; Mamo, A.; Stefio, I.; Di Pietro, C.; Romeo, G.; Campagna, S. *Anal. Chem.* **1998**, *70*(23), 5019–5023.
(26) Caspar, J. V.; Meyer, T. J. *J. Am. Chem. Soc.* **1983**, *105*(17), 5583–5590.
(27) Constable, E. C.; Henney, R. P. G.; Leese, T. A.; Tocher, D. A. *J. Chem. Soc., Dalton Trans.* **1990**, No. 2, 443–449.

reduced pressure, diluted with water (50 mL), and combined with NH_4PF_6 (800 mg). This solution was then concentrated under reduced pressure until the product precipitated and cooled to 5 °C for 16 h. The precipitate was isolated by vacuum filtration, washed with water (2 × 20 mL), and recrystallized from dichloromethane/methanol to give the product as a light red solid (80 mg, 0.10 mmol, 10% yield).

^{1}H NMR (500 MHz, acetone): δ 8.73 (d, J = 8.0, 2H), 8.63 (d, J = 7.5, 2H), 8.43 (d, J = 8.0, 2H), 8.27 (t, J = 8.0, 2H), 8.14 (t, J = 7.0, 2H), 8.08 (d, J = 5.5, 2H), 7.85 (d, J = 8.0, 2H), 7.43 (t, J = 7.0, 2H), 6.89 (t, J = 7.5, 2H), 6.73 (t, J = 7.5, 2H), 6.07 (d, J = 7.5, 2H). ^{13}C NMR (126 MHz, acetone): δ 165.79, 158.09, 154.93, 151.43, 146.79, 145.76, 140.20, 139.13, 131.77, 131.24, 128.28, 126.39, 125.20, 123.08, 120.32, 120.24. MS (ESI, m/z (%)): 655(100), 653(55), 656(34), 654(22). Elem Anal. Calcd for $[IrC_{32}H_{22}N_4]PF_6$: C, 48.06; H, 2.77; N, 7.01. Found: C, 48.16; H, 2.77; N, 6.84.

Hydrogen Evolution Experiments. Samples were prepared in 40 mL precleaned screw cap vials (VWR) through the addition of 750 μL of a 1.33 mM photosensitizer (PS) stock solution in acetone that was subsequently concentrated to dryness under reduced pressure. To this PS charged vial was added 10 mL of a 0.5 M triethylamine (TEA) solution in a 4:1 cosolvent/H_2O mixture (cosolvent = ACN, dimethylformamide (DMF), or tetrahydrofuran (THF)). A palladium catalyst precursor was then added through the addition of 50 μL of an aqueous 6 mM K_2PdCl_4 solution. Each sample was capped with a custom-built lid containing a voltage−pressure transducer (Omega PX-138−030A5 V). The transducers have an operating range of 0−30 psi and were driven in parallel at 8 V using a variable power supply (Tenma 72−6152). The samples were deoxygenated though seven iterations of applying a vacuum and subsequently backfilling with argon. The samples were placed in a 16-sample photoreactor that was illuminated from the bottom by Luxeon V Dental Blue LEDs (LXHL-LRD5) that were driven two in a series at 700 mA using Xitanium drivers (Advance LED120A0700C24F). The LEDs have a maximum emission of 460 nm with a 20 nm full-width at half-maximum (fwhm) and are mounted with collimating optics (Fraen FHS-HNB1-LL01-H) to give 500 ± 50 mW of power to the individual samples. Each LED was affixed to a copper plate that was situated on a water-cooled aluminum block, and the entire setup was agitated at 150 rpm using an orbital shaker (IKA KS 260). Pressure data were collected every second for the first 10 min of the reaction and every 10 s thereafter using a PC interface designed in LabView. Pressure changes due to thermal fluctuations were monitored using a reference vial that contained only the reaction solvent mixture, and these slight variations were subtracted from the pressure traces of the samples. Analysis of the gases was performed using a Hamilton SampleLock syringe and a Standard Research System QMS Series Gas Analyzer that was calibrated using reference standards of 1:9 H_2/Ar and 1:1 H_2/Ar (Airgas).

Computational Details. Density functional theory (DFT) calculations were performed using the Gaussian 03 suite.[28] Ground-state geometries were calculated using the B3LYP functional and the LanL2DZ basis set. Default thresholds for gradient convergence were used while a slightly relaxed threshold for wave function convergence [SCF = (CONVER = 7)] was employed for all calculations. Time-dependent DFT (TD-DFT) calculations were obtained for the optimized ground-state geometry using the conductor polarizable continuum model (C-PCM) present in Gaussian 03 to simulate solvent effects. Calculation of the UV−vis spectra was accomplished using GaussSum 2.1.4[29] with a fwhm of 4000 cm^{-1}.

Results and Discussion

Ground-state DFT calculations of $[Ir(phbpy)_2]^+$ and $[Ir(ppy)_2(bpy)]^+$ reveal similar results for the locations of the highest occupied molecular orbital (HOMO) and the lowest unoccupied molecular orbital (LUMO) of each complex, as shown in Figure 2. For both species, the 95% electron density of the HOMO shows comparable density on the iridium center and the phenyl moieties. In contrast, the LUMO primarily resides on the bpy portion(s) of both complexes, where the LUMO of $[Ir(phbpy)]^+$ is equally distributed over both of the bpy portions of the phbpy ligands. The mixing of the metal and ligand orbitals in the HOMOs of both complexes allows for the formation of a mixed excited state that is comprised of both metal-to-ligand and ligand-centered transitions. As described previously,[1,3,16−18] this property aids in tuning the photophysical properties of the heteroleptic $[Ir(C^\wedge N)_2(N^\wedge N)]^+$ complexes, and similar strategies could be successful in tuning the photophysical properties of the more robust $[Ir(C^\wedge N^\wedge N)_2]^+$ complexes.

The similar DFT results obtained for $[Ir(ppy)_2(bpy)]^+$ and $[Ir(phbpy)_2]^+$ are reflected in the electrochemical properties of the two complexes. $[Ir(phbpy)_2]PF_6$ demonstrates a reversible Ir(III/IV) oxidation wave ($E_{1/2}$ = 1.26 V vs SCE, $\triangle E_p$ = 83 mV) and two reversible reduction waves ($E_{1/2}$ = −1.43 V vs SCE, $\triangle E_p$ = 66 mV and $E_{1/2}$ = −1.67 V vs SCE, $\triangle E_p$ = 67 mV), as shown in Figure 3. These electrochemical characteristics are similar to those of the parent complex $[Ir(ppy)_2(bpy)]PF_6$, which shows a reversible one-electron Ir(III/IV) oxidation wave ($E_{1/2}$ = 1.24 V vs SCE, $\triangle E_p$ = 84 mV) and a reversible one-electron bpy^0/bpy^{-1} reduction wave ($E_{1/2}$ = −1.41 V vs SCE, $\triangle E_p$ = 66 mV). The second reduction wave of $[Ir(phbpy)_2]PF_6$ at a slightly more negative potential is attributed to the fact that the complex effectively has a second bpy subunit that can be reduced.

Unlike the electrochemical behavior, the photophysical properties of $[Ir(phbpy)_2]PF_6$ are notably different from those of $[Ir(ppy)_2(bpy)]PF_6$, as summarized in Table 1. The use of the $C^\wedge N^\wedge N$ ligand allows for a more absorptive and red-shifted predominately MLCT of the $[Ir(phbpy)_2]PF_6$ complex, as shown in Figure 4. This increased absorptivity of the $[Ir(phbpy)_2]PF_6$ complex relative to $[Ir(ppy)_2(bpy)]PF_6$ into visible wavelengths was interpreted using TD-DFT and presumably results from both electronic and Franck−Condon factors.[30] Since the majority of terrestrial radiant energy received from the sun is in the visible portion of the spectrum, increased absorption into lower-energy wavelengths will be crucial to the success of similar molecules to be used as

(28) Frisch, M. J.; Trucks, G. W.; Schlegel, H. B.; Scuseria, G. E.; Robb, M. A.; Cheeseman, J. R.; Montgomery, J. A., Jr.; Vreven, T.; Kudin, K. N.; Burant, J. C.; Millam, J. M.; Iyengar, S. S.; Tomasi, J.; Barone, V.; Mennucci, B.; Cossi, M. S. G.; Rega, N.; Petersson, G. A.; Nakatsuji, H.; Hada, M.; Ehara, M.; Toyota, K.; Fukuda, R.; Hasegawa, J.; Ishida, M.; Nakajima, T.; Honda, Y.; Kitao, O.; Nakai, H.; Klene, M.; Li, X.; Knox, J. E.; Hratchian, H. P.; Cross, J. B.; Bakken, V.; Adamo, C.; Jaramillo, J.; Gomperts, R.; Stratmann, R. E.; Yazyev, O.; Austin, A. J.; Cammi, R.; Pomelli, C.; Ochterski, J. W.; Ayala, P. Y.; Morokuma, K.; Voth, G. A.; Salvador, P.; Dannenberg, J. J.; Zakrzewski, V. G.; Dapprich, S.; Daniels, A. D.; Strain, M. C.; Farkas, O.; Malick, D. K.; Rabuck, A. D.; Raghavachari, K.; Foresman, J. B.; Ortiz, J. V.; Cui, Q.; Baboul, A. G.; Clifford, S.; Cioslowski, J.; Stefanov, B. B.; Liu, G.; Liashenko, A.; Piskorz, P.; Komaromi, I.; Martin, R. L.; Fox, D. J.; Keith, T.; Al-Laham, M. A.; Peng, C. Y.; Nanayakkara, A.; Challacombe, M.; Gill, P. M. W.; Johnson, B.; Chen, W.; Wong, M. W.; Gonzalez, C.; Pople, J. A. *Gaussian 03*, revision C.02; Gaussian, Inc.: Wallingford, CT, 2004.

(29) O'Boyle, N. M.; Tenderholt, A. L.; Langner, K. M. *J. Comput. Chem.* **2008**, *29*(5), 839–845.

(30) Turro, N. J. *Modern Molecular Photochemistry*; University Science Books: Sausalito, CA, 1991; pp 76−152.

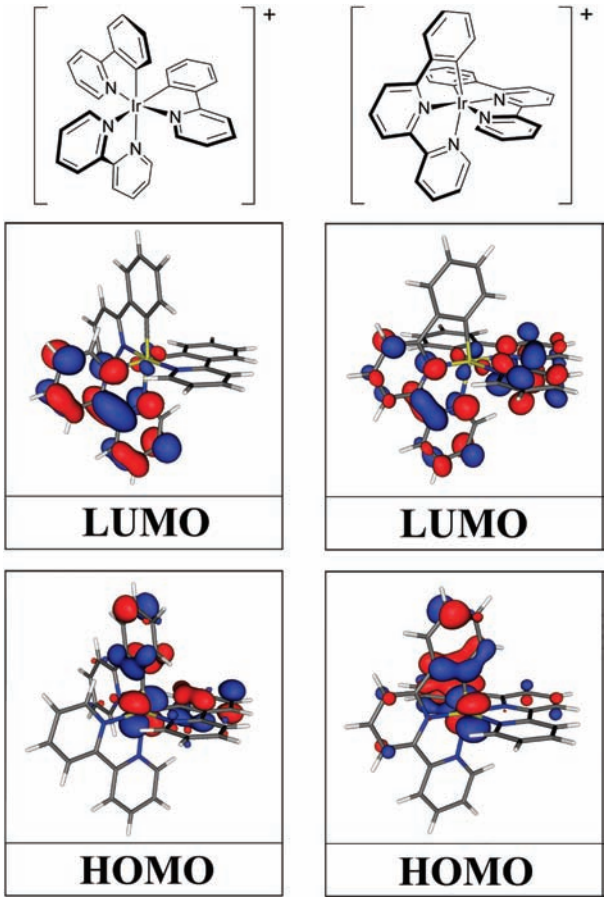

Figure 2. Frontier orbitals of $[Ir(ppy)_2(bpy)]^+$ (left) and $[Ir(phbpy)]^+$ (right) in the singlet ground state obtained through DFT calculations (B3LYP/LanL2DZ). Both calculations reveal similar results in that the HOMO of both complexes is a mixture of orbitals from the metal and the phenyl moieties. The LUMO of both complexes is primarily formed from the bpy moieties, and the LUMO of $[Ir(phbpy)]^+$ is distributed over both of the bpy portions of the phbpy ligands.

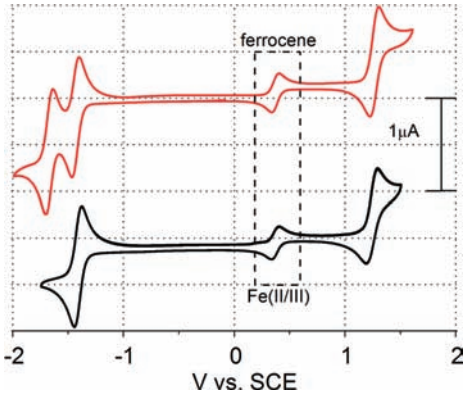

Figure 3. CV of 500 μM solutions of $[Ir(phbpy)_2]PF_6$ (red line, top) and $[Ir(ppy)_2(bpy)]PF_6$ (black line, bottom) performed at a sweep rate of 100 mV/s in 0.1 M TBAH in acetonitrile using a 1 mm^2 platinum disk working electrode, a coiled platinum counter electrode, and a silver wire pseudoreference electrode and containing a ferrocene internal reference.

photosensitizers for solar energy conversion. Additionally, the $[Ir(phbpy)_2]PF_6$ complex in acetonitrile has an increased excited-state lifetime (τ) of 548 ns compared to the 385 ns lifetime of $[Ir(ppy)_2(bpy)]PF_6$. This longer excited-state lifetime is presumably due to the increased rigidity of the *bis*-C^N^N complex compared to that of the $[Ir(C^N)_2(N^N)]^+$

Table 1. Summary of Photophysical Properties of $[Ir(phbpy)_2]PF_6$ Compared to the Parent Complex $[Ir(ppy)_2(bpy)]PF_6$ in ACN Solutions[a]

	$[Ir(ppy)_2(bpy)]PF_6$	$[Ir(phbpy)_2]PF_6$
ε_{460} ($M^{-1}cm^{-1}$)	711	1235
max $\lambda_{emission}$ (nm)	582	580
τ (ns)	385	548
Φ_{em} (%)	7.3	3.9

[a] Reported values are the average of duplicate measurements, which varied by less than 5% from the result. Molar absorptivity data at the peak emission of the LEDs (ε_{460}) used for catalytic proton reduction were calculated from 400 μM solutions. The emission and lifetime data were acquired using 20 μM solutions.

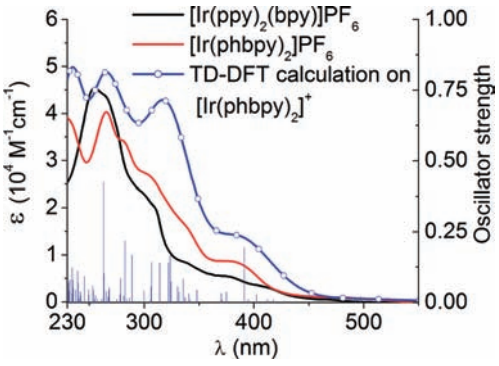

Figure 4. UV−vis absorption spectrum of $[Ir(phbpy)_2]PF_6$ (red line, left axis) compared to that of $[Ir(ppy)_2(bpy)]PF_6$ (black line, left axis) acquired in ACN at a 20 μM concentration. The calculated absorption spectrum (blue line with open symbols, left axis) and oscillator strengths (vertical blue lines, right axis) of $[Ir(phbpy)_2]PF_6$ in ACN is obtained by TD-DFT using the C-PCM present in Gaussian 03 to simulate solvent effects.

species. Notably, the use of the tridentate phbpy ligand slightly lowers the quantum yield of luminescence of $[Ir(phbpy)_2]PF_6$ when compared to $[Ir(ppy)_2(bpy)]PF_6$. The lowered quantum yield may result from a deviation from octahedral geometry of $[Ir(phbpy)_2]PF_6$ and is less dramatic than the comparison of $[Ru(bpy)_3]^{2+}$ ($\Phi_{em} = 6.2\%$) to $[Ru(tpy)_2]^{2+}$ that is practically nonemissive at room temperature.[19,31,32]

Hydrogen Evolution Experiments. In previous studies of hydrogen-evolving systems utilizing a $[Ir(ppy)_2(bpy)]PF_6$ chromophore and a colloidal platinum catalyst in a 9:3:1 ACN/H_2O/triethanolamine solution, it was discovered that bpy dissociation from the complex was correlated with a loss in catalytic activity.[33] Additionally, it was determined that the addition of more PS to a compromised system did not regenerate the catalytic conditions, leading to the conclusion that the platinum catalyst was also deteriorating. However, when the reaction conditions are changed to use a colloidal palladium catalyst and TEA as a sacrificial reductant, sequential PS additions to the compromised system regenerate the catalytic conditions and produce H_2.[34] These improved conditions could be exploited if a more robust photosensitizer were

(31) Young, R. C.; Nagle, J. K.; Meyer, T. J.; Whitten, D. G. *J. Am. Chem. Soc.* **1978**, *100*(15), 4773–4778.
(32) Winkler, J. R.; Netzel, T. L.; Creutz, C.; Sutin, N. *J. Am. Chem. Soc.* **1987**, *109*(8), 2381–2392.
(33) Tinker, L. L.; McDaniel, N. D.; Curtin, P. N.; Smith, C. K.; Ireland, M. J.; Bernhard, S. *Chem.—Eur. J.* **2007**, *13*(31), 8726–8732.
(34) Curtin, P. N.; Tinker, L. L.; Burgess, C. M.; Cline, E. D.; Bernhard, S. *Inorg. Chem.* **2009**, DOI: 10.1021/ic9007763.

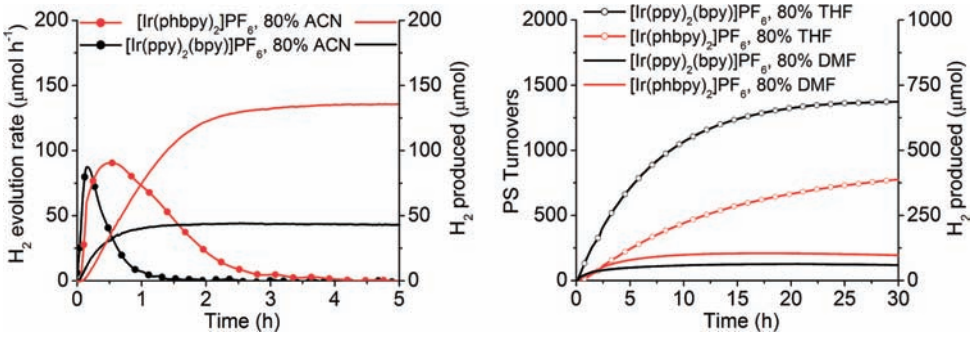

Figure 5. Photocatalytic H_2 evolution from systems utilizing a $[Ir(phbpy)_2]PF_6$ (red lines) or $[Ir(ppy)_2(bpy)]PF_6$ (black lines) PS. Each sample contained 1 μmol of PS and 0.30 μmol of K_2PdCl_4 in 10.0 mL of a 0.5 M TEA solution in a 4:1 cosolvent/H_2O mixture and were illuminated from the bottom using a LED assembly with a maximum emission of 460 nm and a 500 ± 50 mW total power output. Left: H_2 evolution (solid lines, right axis) and rate of H_2 evolution (dotted lines, left axis) for $[Ir(phbpy)_2]PF_6$ (red) and $[Ir(ppy)_2(bpy)]PF_6$ (black) photosensitizers in 4:1 ACN/H_2O. Right: H_2 evolution (right axis) and PS turnovers (left axis) for both photosensitizes when ACN is replaced by THF (open symbols) or DMF (solid lines).

developed, and when the $[Ir(phbpy)_2]PF_6$ complex is used in such conditions, a significant enhancement is observed relative to the $[Ir(ppy)_2(bpy)]PF_6$ photosensitizer (Figure 5). The system using the $[Ir(phbpy)_2]PF_6$ chromophore displayed an almost identical catalytic rate of H_2 evolution but transferred a total of 273 reductive equivalents per PS where the $[Ir(ppy)_2(bpy)]PF_6$-based system only achieved 86 PS turnovers. The increased performance when $[Ir(phbpy)_2]PF_6$ is used as a photosensitizer is a result of the fact that the $[Ir(phbpy)_2]PF_6$ system sustained catalytic activity for approximately 3 times as long as the $[Ir(ppy)_2(bpy)]PF_6$ system. This is easily visualized in the time-resolved rate of hydrogen evolution of both samples shown in Figure 5 (dotted lines). In these time-resolved rate data, it is clear that both catalytic conditions have identical maximum rates of hydrogen evolution of 85 μmol h^{-1}, but the decay of this rate is significantly slowed for the $[Ir(phbpy)_2]PF_6$ photosensitizer.

As catalytic systems that reduce water must have water as a component of the reaction media, the ligating ability of the solvent will continue to promote PS decomposition in similar catalytic cycles. Therefore, the stability of the $[Ir(phbpy)_2]PF_6$ photosensitizer under photocatalytic conditions using an ACN cosolvent is of considerable importance. However, as a result of PS stability being affected by ligating solvents, one of the successful approaches to stabilizing the $[Ir(C^{\wedge}N)_2(N^{\wedge}N)]^+$ chromophores in such catalytic systems is to select nonligating cosolvents such as DMF and THF. The use of DMF and THF presumably minimizes bpy dissociation while also affecting electron-transfer rates due to the differing dielectric constants of the solvent mixtures.[35] The increased performance is dramatic for $[Ir(ppy)_2(bpy)]PF_6$, which only provides 86 PS turnovers in a system utilizing 1 μmol of PS and a Pd colloidal catalyst in 0.5 M TEA in a 4:1 ACN/H_2O mixture, as the THF system is capable of over 1350 PS turnovers and the DMF system demonstrates 125 PS turnovers (PS turnovers = reductive equivalents transferred). However, the 3-fold increase in production that is observed for $[Ir(phbpy)_2]PF_6$ compared to $[Ir(ppy)_2(bpy)]PF_6$ in the ACN-containing system is reduced to a 1.7-fold increase (104 μmol of H_2 produced by 1 μmol of $[Ir(phbpy)_2]PF_6$) when DMF is used as a cosolvent. Additionally, the THF-based system using $[Ir(phbpy)_2]PF_6$ is only capable of producing 410 μmol of H_2, which is a 40% reduction when compared to the analogous $[Ir(ppy)_2(bpy)]PF_6$ system. Although the net amount of hydrogen produced is reduced when the $[Ir(phbpy)_2]PF_6$ complex is used in a 4:1 THF/H_2O mixture, the lifetime of the system is actually increased, as demonstrated in Figure 5 (right). The catalytic conditions employing the $[Ir(ppy)_2(bpy)]PF_6$ photosensitizer produce more hydrogen than the system with $[Ir(phbpy)_2]PF_6$ due to an increased maximum rate of H_2 production. The observed rate increase may result from a specific interaction of the PS with either the colloid or sacrificial reductant (TEA), which is being hindered for $[Ir(phbpy)_2]PF_6$ in this solvent mixture that has a lower dielectric constant than the conditions using DMF or ACN. However, after approximately 12 h, the parent system using $[Ir(ppy)_2(bpy)]PF_6$ no longer produces H_2, where the $[Ir(phbpy)_2]PF_6$ PS continues to evolve H_2 for over 30 h, reaffirming the supposition that the $C^{\wedge}N^{\wedge}N$ ligand architecture provides a more stable photosensitizer.

Conclusions

A novel complex of iridium(III) using a tridentate $C^{\wedge}N^{\wedge}N$ ligand was synthesized and compared to its well-studied $[Ir(ppy)_2bpy]PF_6$ counterpart. The *bis*-cyclometalated $[Ir(C^{\wedge}N^{\wedge}N)_2]^+$ complex demonstrates similar electrochemical properties, and DFT calculations reveal that the successful tuning strategies of $[Ir(C^{\wedge}N)_2(N^{\wedge}N)]^+$ complexes could be used in tuning the excited states of the reported $[Ir(C^{\wedge}N^{\wedge}N)_2]^+$ architecture. The photophysical and electrochemical properties of the $[Ir(phbpy)_2]PF_6$ complex were studied, revealing a second reductive wave as a result of the second bpy subunit and an increased lifetime of luminescence compared to $[Ir(ppy)_2(bpy)]PF_6$. Additionally, the novel complex was employed in systems that catalytically reduce protons, and the increased stability of the $[Ir(phbpy)_2]PF_6$ chromophore was demonstrated. The synthesis of $[Ir(C^{\wedge}N^{\wedge}N)_2]^+$ allows one to exploit the advantages of *bis*-tridentate complexes relative to their *tris*-bidentate counterparts for the versatile $[Ir(C^{\wedge}N)_2(N^{\wedge}N)]^+$ framework.

Acknowledgment. The authors would like to thank Eric Cline, Neal McDaniel, and Christine Burgess for their useful discussions. S.B. acknowledges support through a NSF CAREER award (CHE-0449755).

(35) Cline, E. D.; Adamson, S. E.; Bernhard, S. *Inorg. Chem.* **2008**, *47*(22), 10378–10388.